JCTC Journal of Chemical Theory and Computation

Article

pubs.acs.org/JCTC

Electronic Quenching in $N(^2D) + N_2$ Collisions: A State-Specific Analysis via Surface Hopping Dynamics

B. R. L. Galvão,[†] J. P. Braga,[‡] J. C. Belchior,*[,‡] and A. J. C. Varandas*[,§]

[†]Departmento de Química, Centro Federal de Educacão Tecnológica de Minas Gerais, CEFET-MG, Av. Amazonas 5253, 30421-169, Belo Horizonte, Minas Gerais, Brazil

[‡]Departamento de Química-ICEx, Universidade Federal de Minas Gerais, Av. Antônio Carlos 6627, Pampulha, 31270-901, Belo Horizonte, Minas Gerais, Brazil

[§]Departamento de Química, Universidade de Coimbra, 3004-535 Coimbra, Portugal

ABSTRACT: The electronic quenching reaction $N(^2D) + N_2 \rightarrow N(^4S) + N_2$ is studied using the trajectory surface hopping method and employing two doublet and one quartet accurate potential energy surfaces. State-specific properties are analyzed, such as the dependence of the cross section on the initial quantum state of the reactants, vibrational energy transfer, and rovibrational distribution of the product N_2 molecule in thermalized conditions. It is found that rotational energy on the reactant N_2 molecule is effective in promoting the reaction, whereas vibrational excitation tends to reduce the reaction probability. For initial states and collision energy thermalized in an initial bath, it is found that the products are "hotter", both vibration and rotation wise.

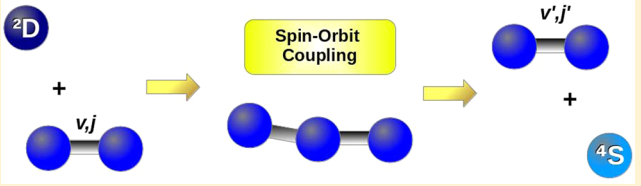

1. INTRODUCTION

Nitrogen atom in its excited ^2D state plays an important role in the ionosphere due to the reaction

$$N(^2D) + O_2 \rightarrow NO + O \quad (1)$$

which is the major source of nitric oxide.[1] By converting kinetic energy into radiation in the infrared region, NO plays a fundamental role in the cooling mechanism of the atmosphere.[2,3] The reactions that deactivate $N(^2D)$ to its ground state, such as[4]

$$N(^2D) + O \rightarrow N(^4S) + O \quad (2)$$

$$N(^2D) + N_2 \rightarrow N(^4S) + N_2 \quad (3)$$

will therefore have an influence on the amount of NO available. In fact, these reactions generate $N(^4S)$, which removes atmospheric NO[5,6] via $N(^4S) + NO \rightarrow N_2 + O(^3P)$ and hence are important in the study of nitric oxide abundance.

Multiple experiments have been carried out for obtaining the rate constant of reaction 3,[7−13] but the temperature dependences obtained by different groups do not agree with each other, as summarized in ref 14. Despite the controversy on a precise value, it is generally accepted that this rate constant is very small compared to that of reaction 2, and therefore the title reaction is normally neglected. In a recent letter[15] we have addressed this assumption theoretically, contributing to understanding and solving the discrepancies in the experimental results, while also elucidating at what altitudes this reaction can be in fact neglected. In the present work we focus on the state specific rate constants and cross sections, including an analysis of the ro-vibrational distribution of the products and the dependence of the reaction probability on the initial quantum states of the N_2 molecule. This problem involves at least two doublet and one quartet potential energy surfaces (PESs), in global analytic form, to be used in the quasiclassical dynamics involving electronic spin-forbidden dynamics.

2. METHODOLOGY

2.1. Potential Energy Surfaces. The interaction of the $N(^2D)$ atom with N_2 gives rise to five PESs, of which only two are attractive. For the quartet state, only the $N_3(^4A'')$ PES correlates with the $N(^4S) + N_2$ channel, which is repulsive and shows several crossings with the doublet ones. Accurate ab initio based PESs employing the double many-body expansion (DMBE) method[16−18] have been proposed for the trinitrogen system,[19−21] which show systematic accuracy and are the first set of potentials that can be applied to study the title electronic quenching reaction.

Such PESs reproduce all important features of the title system and are represented in Figure 1 for a linear attack of the N atom to N_2 with its bond length relaxed for the lowest energy. The two lowest doublet states ($1^2A'$ and $1^2A''$) are degenerate for linear configurations, which include the global minimum corresponding to the N_3 molecule in its $^2\Pi_g$ state. The transition state (TS) shown in Figure 1 corresponds to the lowest energy barrier for reaching the covalent region from the $N(^2D) + N_2$ channel and is also degenerate for both doublet states, lying 2.8 kcal mol^{-1} above the reactants channel.[22]

The highest probability for an intersystem crossing, leading to the quenched $N(^4S)$ product, occurs on the regions of the PES where the quartet state crosses the doublet ones. Figure 1

Received: February 4, 2014
Published: April 7, 2014

   dx.doi.org/10.1021/ct500085q | J. Chem. Theory Comput. 2014, 10, 1872−1877

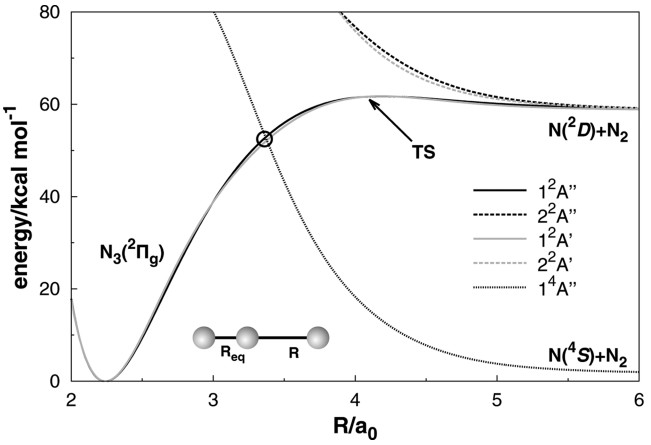

Figure 1. Optimized linear path for a N atom approach to a N_2 molecule, showing the ground and excited $^2A''$ states (black lines), the $^2A'$ states (gray), and the quartet one (black dotted line). The ⊙ symbol corresponds to a crossing between the quartet and doublet PESs.

shows an example in the minimum energy path for reaction, but there are other crossing regions for other nuclear arrangements. Morokuma and co-workers[22] have optimized the minimum on these doublet/quartet crossings seams and calculated the norm of the spin−orbit (SO) coupling matrix elements as

$$V_{SO} = \langle D|H^{SO}|Q\rangle \tag{4}$$

where $|D\rangle$ and $|Q\rangle$ stand for the doublet and quartet electronic wavefuntions, respectively. These values will be used to calculate transition probabilities in the dynamics studies reported in the next section.

It is very insightful to plot the PESs in hyperspherical coordinates, relaxing the perimeter of the triangle formed by the atoms such as to minimize the energy for each "shape" of the molecule. This is performed with the relaxed triangular plot[23] using the scaled coordinates, $\beta^* = \beta/Q$ $\gamma^* = \gamma/Q$:

$$\begin{pmatrix} Q \\ \beta \\ \gamma \end{pmatrix} = \begin{pmatrix} 1 & 1 & 1 \\ 0 & \sqrt{3} & -\sqrt{3} \\ 2 & -1 & -1 \end{pmatrix} \begin{pmatrix} {R_1}^2 \\ {R_2}^2 \\ {R_3}^2 \end{pmatrix} \tag{5}$$

This graph is shown in Figure 2, where the doublet PESs $^2A'$ and $^2A''$ are displayed superposed with the quartet one. The equilateral triangle (D_{3h}) geometry is located at the center of the plot ($\gamma^* = \beta^* = 0$), and a pseudorotation is obtained when performing a loop around this point. Also, linear configurations lie on the border of the limiting circle, and C_{2v} structures are found under the lines that would divide the circle in six equivalent pieces. For a quick visual guide on how to interpret the graph, the reader is addressed to ref 21, where such plots are accompanied by a geometric representation of the stationary points on the N_3 PESs (see also ref 24 for an analogous representation). Note that the doublet/quartet crossing seams are now in evidence, and the minima on the crossing seam predicted by Morokuma and co-workers[22] are shown with a blue point.

2.2. Trajectory Surface Hopping Dynamics. The quasiclassical trajectories employed here follow the method of ref 15. Briefly, for a given initial rovibrational state of the N_2 molecule and relative translational energy, the impact parameter, orientation of the reactants, momentum, and phase of the reactant diatomic molecule are sampled according to their probability distribution using the QCT method.[25,26] The calculation starts on a doublet PES, and the integration of Hamilton's equations of motion is performed with a time step of 0.1 fs.

In order to account for electronic transitions, the trajectory surface hopping[27−29] (TSH) method is applied as implemented in ref 30. In this method the trajectory is followed at each integration step to check if a doublet/quartet crossing has been passed, in which case one gets back one integration step and restarts the process with a time step 200 times smaller to find more precisely the crossing point. The Landau−Zenner transition probability for diabatic surfaces is then calculated according to[30,31]

$$P_{LZ} = 1 - \exp\left(\frac{-2\pi {V_{SO}}^2}{\hbar|\Delta F v|}\right) \tag{6}$$

where ΔF is the difference in forces between the two surfaces and v the velocity, both evaluated at the crossing point in the direction normal to the crossing seam.

The values ascribed to V_{SO} are taken from ref 22 and are not a function of the internuclear distances but rather a fixed value set for each region around the minimum of that particular crossing seam. A random number ξ is generated between 0 and 1, and if $P_{LZ} > \xi$ a hop occurs and the integration of the classical equations of motion proceeds in the new surface.

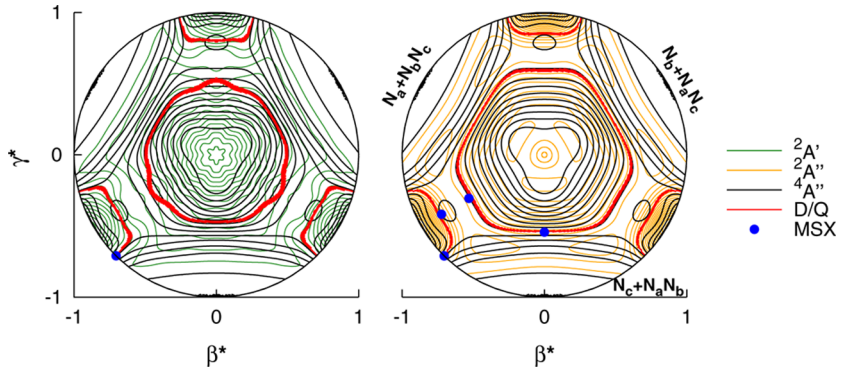

Figure 2. Relaxed triangular plot in hyperspherical coordinates.[23] The $^2A'$ and $^2A''$ PES are shown separately and superposed to the $^4A''$ one. The red lines indicate the seam of doublet/quartet crossing, and the blue points correspond to the minima on the crossing seam (MSX) predicted by Morokuma and co-workers.[22]

dx.doi.org/10.1021/ct500085q | J. Chem. Theory Comput. 2014, 10, 1872−1877

The use of quasiclassical trajectories is justified for this system, given the mass of the nitrogen atoms. It has been shown[32] for $N(^4S) + N_2$ that quasiclassical trajectories are capable of achieving the same accuracy as the quantum mechanical treatment if one is interested only in averaged properties such as rate constants. A further approximation is that the $^2A'$ and $^2A''$ surfaces are considered to be decoupled and no transition between them is allowed. In fact, what is observed is that after hopping to the quartet state the system experiences a strong gradient toward dissociation (see Figure 1) and quickly forms products with no secondary hops.

After running a large number of trajectories N, the Monte Carlo integrated rate constant is given by

$$\sigma_x = \pi b_{\max}^2 \frac{N_r}{N} \tag{7}$$

with the final result being given by $\sigma = \sigma_{^2A'\rightarrow{}^4A''} + \sigma_{^2A''\rightarrow{}^4A''}$. In the above equation, $b_{\max}$ is the maximum value of the impact parameter which has been optimized by trial and error such as to guarantee that no trajectory will be reactive with a larger b value and N_r is the number of trajectories that hopped to the quartet state and ended up with the quenched $N(^4S)$ atom, either via exchanging nitrogen atoms with the diatomic or not. The associated 68% error bars are given by $\Delta\sigma_x = \sigma_x((N - N_r)/(NN_r))^{1/2}$.

In a second part of the analysis, instead of fixed values of translational energy and initial quantum numbers, we simulate atmospheric conditions by sampling these variables using their probability distribution for a given temperature, while taking into consideration the appropriate ortho-para symmetry weights for the initial rotational population of the N_2 diatomic. Although there are grounds to believe that thermalization cannot be easily achieved in the middle and high regions of the atmosphere,[33] we will carry such calculations assuming a thermal distribution of these variables as sampled by the Monte Carlo method. Given that very few trajectories will have enough total energy to overcome the reaction barrier, we have employed the quantum mechanical threshold[34] (QMT) method, where only trajectories that show enough total energy to reach the zero-point energy (ZPE) of the transition state are integrated; all others are considered as nonreactive. In order to obtain the population of the rovibrational levels of the product molecule, its internal energy is quantized for each trajectory using the semiclassical quantization method.[26]

3. RESULTS AND DISCUSSION

3.1. Excitation Function. As mentioned above, the cross sections for the electronic quenching reaction must be calculated separately for the $^2A'$ and $^2A''$ initial states, and Figure 3 shows each contribution for collisions on the ground rovibrational state of N_2 (black lines). For low collision energies, the two contributions are seen to be similar, which is due to the fact that the minimum energy path for overcoming the TS is collinear and is degenerate for both surfaces (see Figure 1). However, the $^2A'$ sheet is more repulsive for bent configurations and differs largely from the $^2A''$ one.[21] Therefore, different configurations are available for higher energies, and the $^2A''$ reactivity gets enhanced as seen in Figure 3.

Labeling each nitrogen atom, a collision process can be described as $N_a(^2D) + N_bN_c$, while the total quenching cross section encompasses three reactive channels, namely, $N_a(^4S) + N_bN_c$, $N_b(^4S) + N_aN_c$ and $N_c(^4S) + N_aN_b$. In this way, we also discriminate the portion of the total rate constant that

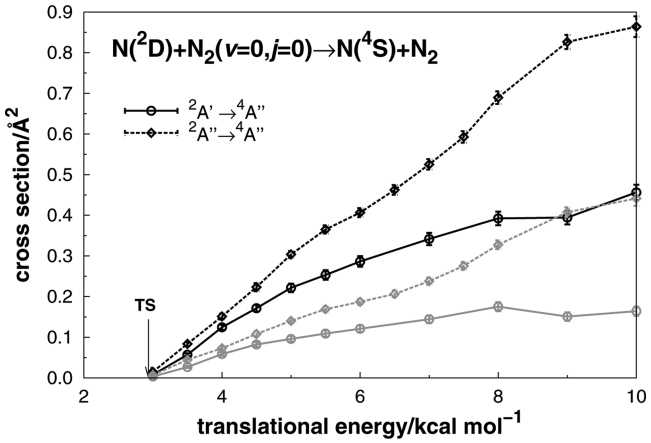

Figure 3. Contributions from each initial doublet symmetry for the total reaction cross section (black) and for the cross section of quenching and exchanging nitrogen atoms (gray). The energy of the transition state (including ZPE correction) is highlighted with an arrow.

corresponds to formation of the quenched atom with an exchange taking place with the diatomic. This is shown for both initial doublet PESs in Figure 3 (gray lines), which indicates that these exchanged trajectories correspond roughly to half of the total number.

The total cross section for different rovibrational levels of the reactant molecule is presented in Figure 4 as a sum of the two

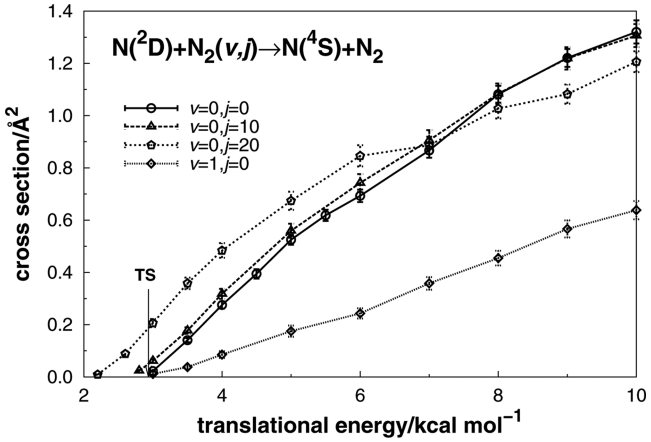

Figure 4. Total reaction cross section for selected initial rovibrational states of the reactant molecule.

initial doublet PESs and without discriminating exchanged trajectories. We have previously argued[20] that the $N(^2D)-N_2$ approach shows an early barrier, which in the context of the Polanyi rules would suggest that vibrational energy is not effective for promoting the reaction. In fact, as can be seen in Figure 4, vibrational excitation on the entrance channel reduces significantly the reaction cross section, without changing the threshold for translational energy, and thus the Polanyi rules hold for the present case. However, this level lies 6.5 kcal mol^{-1} above the ZPE of N_2 and is barely populated even for temperatures as high as 1000 K. The impact of vibrationally excited states should therefore be small under thermal equilibrium but may play a different role for nitrogen containing plasmas and extreme atmospheric conditions.[35−37]

Rotationally excited states on the other hand are populated under ordinary temperatures and are also show in Figure 4 for $v = 0$, $j = 10$ and $v = 0$, $j = 20$, which lie 0.6 and 2.4 kcal mol^{-1} above the N_2 ZPE, respectively. Note that the $(2j + 1)$ degeneracy of each level is not multiplied and thus the contributions from these states are higher than shown in this graph. It is interesting to note that rotational energy not only increases the cross-section but also reduces the threshold of translational energy to values even below the barrier. This seems to suggest that rotational energy can be partially exchanged when the two reactants approach each other outside the covalent region and hence help overcoming the reaction TS.

3.2. Vibrational to Vibrational Energy Transfer. The energy transfers that take place in collisions between atomic and molecular nitrogen are important for the study of extreme conditions, such as high-speed entry of a spacecraft into the Earth's atmosphere,[38] and also in nonequilibrium kinetics of nitrogen and air plasmas.[39] Given that excited electronic states may be important in these cases,[36,37] it is desirable to include $N(^2D)$ in the analysis. After obtaining our set of PESs[19−21] for $N(^2D) + N_2$ interactions, it became possible to study such energy transfer processes.

Given that intersystem crossings present very low probability, one could, as a first approach, ignore the doublet/quartet transitions in the atom−diatom energy transfer process. This was performed in ref 40, where for fixed initial vibrational states of N_2, we have sampled rotational and translational energies from a thermal distribution for temperatures in the range of $750 \leq T$ (K) ≤ 1250. The results for $T = 750$ K are shown in the top panel of Figure 5, where it is seen that deactivation is by far the most probable event. In this work we have repeated these calculations, but now allowing for hops between the doublets and quartet states, and the bottom panel of Figure 5 shows the rate constant for electronic quenching via $v_i \rightarrow v_f$. It is seen that electronic deactivation of $N(^2D)$ may be accompanied by a change in the vibrational state of the diatomic: in this case, vibrational excitation and deactivation have similar probabilities. Furthermore, as shown in the previous section, vibrational excitation on the reactant N_2 decreases considerably the reaction probability, which can also be observed in this figure. The rate constants for $v_i = 0$ largely exceed the ones for higher v_i. The results are given numerically in Table 1.

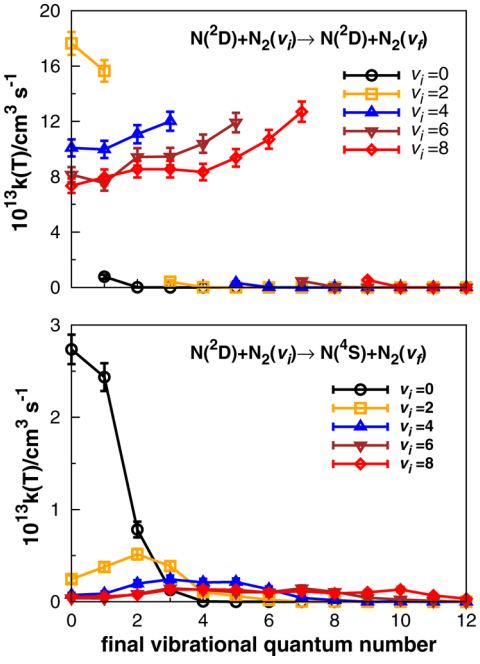

Figure 5. Rate constants for the $v_i \rightarrow v_f$ vibrational energy transfers, with rotation and translational motion thermalized at $T = 750$ K. The top panel shows results without including electronic transitions, while the bottom one refers to quenched trajectories.

Table 1. Rate Constants for the State-to-State Vibrational Energy Transfer (in 10^{14} cm^3 mol^{-1})[a]

v_i/v_f	0	2	4	6	8
0	27.4 ± 1.6	2.4 ± 0.4	0.7 ± 0.2	0.4 ± 0.2	0.5 ± 0.2
1	24.3 ± 1.5	3.8 ± 0.5	0.9 ± 0.2	0.4 ± 0.2	0.6 ± 0.2
2	7.8 ± 0.9	5.1 ± 0.6	2.0 ± 0.4	0.9 ± 0.2	0.8 ± 0.2
3	1.3 ± 0.3	3.9 ± 0.5	2.4 ± 0.4	1.5 ± 0.3	1.3 ± 0.3
4	–	1.1 ± 0.3	2.1 ± 0.4	1.3 ± 0.3	1.3 ± 0.3
5	–	0.6 ± 0.2	2.1 ± 0.4	1.0 ± 0.3	1.3 ± 0.3
6	–	0.2 ± 0.1	1.4 ± 0.3	1.0 ± 0.3	1.0 ± 0.2
7	–	–	0.4 ± 0.2	1.5 ± 0.3	1.1 ± 0.3
8	–	–	0.2 ± 0.1	1.1 ± 0.3	0.9 ± 0.2
9	–	–	–	0.4 ± 0.2	1.0 ± 0.3
10	–	–	–	0.3 ± 0.1	1.3 ± 0.3
11	–	–	–	0.1 ± 0.1	0.7 ± 0.2
12	–	–	–	–	0.3 ± 0.1

[a]The rotation and translation motions are thermalized at $T = 750$ K.

3.3. Thermal Rate Constants and Products Distributions. For simulating atmospheric conditions, thermal equilibrium is assumed and thus the relative translational energy as well as the initial rovibrational state of the diatomic molecule are sampled from their probability distributions at a given temperature. In this way, the final reaction rate constant has been calculated[15] for temperatures in the range of $240 \leq T$ (K) ≤ 1000. The results around room temperature have shown to agree quite well with available experimental data, while also contributing to understand their temperature dependence.[15] In the present work we further explore the thermal reaction by calculating the rate constant for the quenching with exchange of nitrogen atoms, which is shown in Figure 6. The ratio between the two curves is around 0.45, indicating again that the number of nonexchanging trajectories exceed the sum of the two other channels.

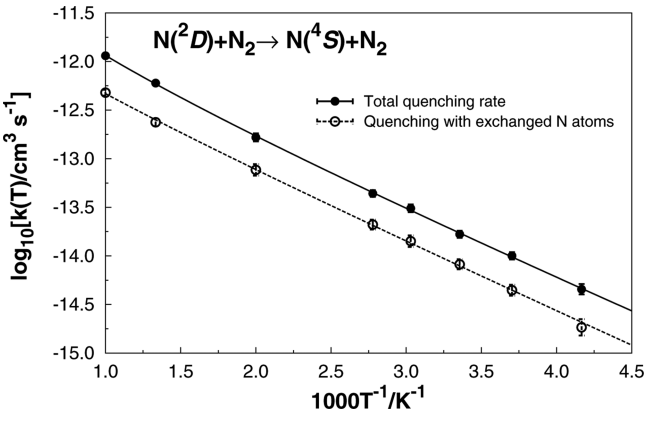

Figure 6. Arrhenius plot of the thermal rate constants.

dx.doi.org/10.1021/ct500085q | J. Chem. Theory Comput. 2014, 10, 1872−1877

After calculating these batches of trajectories for fixed temperatures, we focus on the analysis of the energy distribution of the products, which are expected to be "hotter" since the difference in potential energy from reactants to products (the nitrogen $^2D/^4S$ gap) must be converted to kinetic energy among the available degrees of freedom. As seen in Figure 7, the vast majority of the nitrogen molecules in thermal

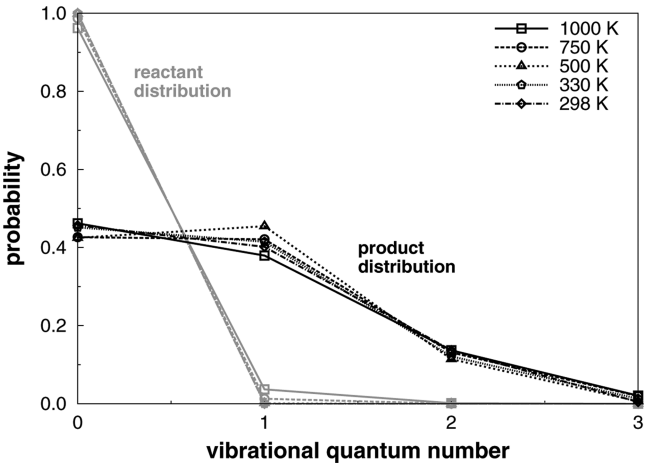

Figure 7. Vibrational distribution on the reactant and product diatomic molecule for the thermalized reaction.

equilibrium are in the ground vibrational state even for the highest temperature of 1000 K, but the distribution of the product molecule is largely different. The population of the first excited vibrational state is similar to the ground one. The second excited state is quite populated as well for all temperatures, exceeding 10% of the total trajectories for all temperatures in the graph.

A similar analysis regarding the rotational states is given in Figure 8 for a temperature of T = 500 K. Since there are many

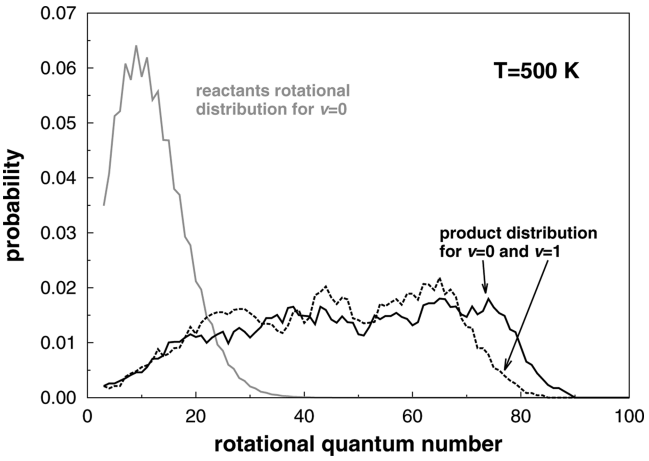

Figure 8. Rotational distribution on the reactant and product diatomic molecule for the batch thermalized at 500 K.

states available, a large number of trajectories must be considered to achieve a smooth curve for the products. For this specific temperature we have employed 150000 trajectories. To obtain a smoother representation, we have followed ref 41, where each data value is replaced by an average of itself and six nearby neighbors, three to the left and three to the right. Note also that the spikes in the initial distribution arise from the ortho-para symmetry weights for N_2. The graph shows the final distribution of rotational levels for collisions that ended up on the ground vibrational state and for those finishing in the first excited one (the two most probable levels, as discussed previously). It is seen that, as for the vibrational case, the products distribution is largely shifted toward excited states. The average rotational level for this temperature is j = 11 for the initial distribution, whereas the final outcome gives 46 for the A' and 43 for the A'' sheet (irrespective of the vibrational state).

Both vibrational and rotational distributions of the products are not changed qualitatively if trajectories that quenched with an exchanged nitrogen atom are analyzed separately, and thus the exchanged products are not formed in a much different way from the total quenching reaction.

4. CONCLUSIONS

State specific reaction cross sections are calculated for the electronic quenching reaction $N(^2D) + N_2 \rightarrow N(^4S) + N_2$. It is concluded that initial rotational excitation of N_2 is efficient in promoting reaction, while vibrational excitation reduces significantly the reaction probability.

The vibrational-to-vibrational energy transfer process is analyzed, with the adiabatic channel $N(^2D) + N_2(v_i) \rightarrow N(^2D) + N_2(v_f)$ showing rate constants about 1 order of magnitude larger than the corresponding spin-forbidden transition. Additionally, unlike the adiabatic case, the spin-forbidden process shows similar probabilities for vibrational deactivation and excitation.

For the thermalized process, large batches of trajectories are analyzed to obtain the energy distribution of the products $N(^4S) + N_2(v, j)$. It is seen that large rotational−vibrational excitations are observed in the product diatomic, which may reach thermal equilibrium upon subsequent collisions with other molecules in the atmosphere.

AUTHOR INFORMATION

Corresponding Authors

*E-mail: jadson@ufmg.br (J.C.B.).
*E-mail: varandas@qtvs1.qui.uc.pt (A.J.C.V.).

Notes

The authors declare no competing financial interest.

ACKNOWLEDGMENTS

BRLG thanks the Conselho Nacional de Desenvolvimento Científico e Tecnológico (CNPq) for Grant 150071/2013-2. The authors also acknowledge the financial support from CNPq and Fundação de Amparo à Pesquisa do estado de Minas Gerais (FAPEMIG). The support from Fundação para a Ciência e Tecnologia, Portugal, to one of us (A.J.C.V.) is also gratefully acknowledged.

REFERENCES

(1) Duff, J. W.; Sharma, R. D. Quasiclassical Trajectory Study of NO Vibrational Relaxation by Collisions with Atomic Oxygen. *J. Chem. Soc. Faraday Trans.* **1997**, *93*, 2645−2649.

(2) Kockarts, G. Nitric-Oxide Cooling in the Terrestrial Thermosphere. *Geophys. Res. Lett.* **1980**, *7*, 137−140.

(3) Zachor, A. S.; Sharma, R. D.; Nadile, R. M.; Stair, A. T. Inversion of a Spectrally Resolved Limb Radiance Profile for the NO Fundamental-Band. *J. Geophys. Res.* **1985**, *90*, 9776−9782.

(4) Tohmatsu, T. *Compendium of Aeronomy*; Kluwer Academy Publishers: Holland, 1990.
(5) Piper, L. G. The Rate Coefficient for Quenching $N(^2D)$ by $O(^3P)$. *J. Chem. Phys.* **1989**, *91*, 3516−3524.
(6) Fensen, C. G.; Gérard, J.-C.; Rusch, D. W. Rapid Deactivation of $N(^2D)$ by O: Impact on Thermospheric and Mesospheric Odd Nitrogen. *J. Geophys. Res.* **1989**, *94*, 5419−5426.
(7) Black, G.; Slanger, T. G.; John, G. A. S.; Young, R. A. Vacuum-Ultraviolet Photolysis of N_2O. IV. Deactivation of $N(^2D)$. *J. Chem. Phys.* **1969**, *51*, 116−121.
(8) Lin, C.-L.; Kaufman, F. Reactions of Metastable Nitrogen Atoms. *J. Chem. Phys.* **1971**, *55*, 3760−3770.
(9) Husain, D.; Kirsch, L. J.; Wiesenfeld, J. R. Collisional Quenching of Electronically Excited Nitrogen Atoms, $N(2^2D_j 2^2P_j)$ by Time-resolved Atomic Absorption Spectroscopy. *Faraday Discuss. Chem. Soc.* **1972**, *53*, 201−210.
(10) Husain, D.; Mitra, S. K.; Young, A. N. Kinetic Study of Electronically Excited Nitrogen Atoms, $N(2^2D_j 2^2P_j)$, by Attenuation of Atomic Resonance Radiation in the Vacuum Ultra-violet. *J. Chem. Soc. Faraday Trans.* **1974**, *70*, 1721−1731.
(11) Slanger, T. G.; Black, G. Quenching of $N(^2D)$ by N_2 and H_2O. *J. Chem. Phys.* **1976**, *64*, 4442−4444.
(12) Sugawara, K.; Ishikawa, Y.; Sato, S. The Rate Constants of the Reactions of the Metastable Nitrogen-Atoms, ^2D and ^2P, and the Reactions of $N(^4S)+NO \rightarrow N_2+O(^3P)$ and $O(^3P)+NO+M \rightarrow NO_2+M$. *Bull. Chem. Soc. Jpn.* **1980**, *53*, 3159−3164.
(13) Suzuki, T.; Shihira, Y.; Sato, T.; Umemoto, H.; Tsunashima, S. Reactions of $N(^2D)$ and $N(^2P)$ with H_2 and D_2. *J. Chem. Soc. Faraday Trans.* **1993**, *89*, 995−999.
(14) Herron, J. T. Evaluated Chemical Kinetics Data for Reactions of $N(^2D)$, $N(^2P)$, and $N_2(A^3\sum_u^+)$ in the Gas Phase. *J. Phys. Chem. Ref. Data* **1999**, *28*, 1453−1483.
(15) Galvão, B. R. L.; Varandas, A. J. C.; Braga, J. P.; Belchior, J. C. Electronic Quenching of $N(^2D)$ by N_2: Theoretical Predictions, Comparison with Experimental Rate Constants, and Impact on Atmospheric Modeling. *J. Phys. Chem. Lett.* **2013**, *4*, 2292−2297.
(16) Varandas, A. J. C. A General Approach to the Potential Energy Function of Small Polyatomic Systems: Molecules and vdW Molecules. *J. Mol. Struct. Theochem.* **1985**, *21*, 401−424 (The article has been published as part of Vol. 120 of the same journal).
(17) Varandas, A. J. C. Intermolecular and Intramolecular Potentials: Topographical Aspects, Calculation, and Functional Representation via a DMBE Expansion Method. *Adv. Chem. Phys.* **1988**, *74*, 255−338.
(18) Varandas, A. J. C. In *Lecture Notes in Chemistry*; Laganà, A., Riganelli, A., Eds.; Springer: Berlin, 2000; Vol. 75, p 33.
(19) Galvão, B. R. L.; Varandas, A. J. C. Accurate Double Many-Body Expansion Potential Energy Surface for N_3 from Correlation Scaled Ab Initio Energies with Extrapolation to the Complete Basis Set Limit. *J. Phys. Chem. A* **2009**, *113*, 14424−14430.
(20) Galvão, B. R. L.; Varandas, A. J. C. Ab Initio Based Double-Sheeted DMBE Potential Energy Surface for $N_3(^2A'')$ and Exploratory Dynamics Calculations. *J. Phys. Chem. A* **2011**, *115*, 12390−12398.
(21) Galvão, B. R. L.; Caridade, P. J. S. B.; Varandas, A. J. C. $N(^4S/^2D)+N_2$: Accurate Ab Initio-Based DMBE Potential Energy Surfaces and Surface-Hopping Dynamics. *J. Chem. Phys.* **2012**, *137*, 22A515.
(22) Zhang, P.; Morokuma, K.; Wodtke, A. M. High-level Ab Initio Studies of Unimolecular Dissociation of the Ground-State N_3 Radical. *J. Chem. Phys.* **2005**, *122*, 014106.
(23) Varandas, A. J. C. A useful triangular plot of triatomic potential energy surfaces. *Chem. Phys. Lett.* **1987**, *138*, 455.
(24) Babikov, D.; Zhang, P.; Morokuma, K. Cyclic-N_3. I. An accurate potential energy surface for the ground doublet electronic state up to the energy of the $^2A_2/^2B_1$ conical intersection. *J. Chem. Phys.* **2004**, *121*, 6743.
(25) Hase, W. L.; Duchovic, R. J.; Hu, X.; Komornicki, A.; Lim, K. F.; Lu, D.; Peslherbe, G. H.; Swamy, K. N.; Linde, S. R. V.; Varandas, A. J. C.; Wang, H.; Wolf, R. J. VENUS96: A General Chemical Dynamics Computer Program. *QCPE Bull.* **1996**, *16*, 43.
(26) Peslherbe, G. H.; Wang, H.; Hase, W. L. Monte Carlo Sampling for Classical Trajectory Simulations. *Adv. Chem. Phys.* **1999**, *105*, 171−201.
(27) Tully, J. C.; Preston, R. K. Trajectory Surface Hopping Approach to Nonadiabatic Molecular Collisions: The Reaction of H^+ with D_2. *J. Chem. Phys.* **1971**, *55*, 562−572.
(28) Zahr, G. E.; Preston, R. K.; Miller, W. H. Theoretical Treatment of Quenching in $O(^1D) + N_2$ Collisions. *J. Chem. Phys.* **1975**, *62*, 1127−1135.
(29) Voronin, A. I.; Marques, J. M. C.; Varandas, A. J. C. Trajectory Surface Hopping Study of the $Li+Li_2$ $(X^1\sum_g^+)$ Dissociation Reaction. *J. Phys. Chem. A* **1998**, *102*, 6057−6062.
(30) Marks, A. J.; Thompson, D. L. A Trajectory Surface-Hopping Study of Mode Specificity in the Predissociation of N_2O. *J. Chem. Phys.* **1991**, *95*, 8056−8064.
(31) Tachikawa, H.; Hamabayashi, T.; Yoshida, H. Electronic-to-Vibrational and -Rotational Energy Transfer in the $O(^1D)+N_2$ Quenching Reaction: Ab Initio MO and Surface-Hopping Trajectory Studies. *J. Chem. Phys.* **1995**, *99*, 16630−16635.
(32) Caridade, P. J. S. B.; Galvão, B. R. L.; Varandas, A. J. C. Quasiclassical Trajectory Study of Atom-Exchange and Vibrational Relaxation Processes in Collisions of Atomic and Molecular Nitrogen. *J. Phys. Chem. A* **2010**, *114*, 6063−6070.
(33) Varandas, A. J. C. Steady-state distributions of O_2 and OH in the high atmosphere, and implications in the ozone chemistry. *J. Phys. Chem. A* **2003**, *107*, 3769−3777.
(34) Truhlar, D. G. Accuracy of Trajectory Calculations and Transition State Theory for Thermal Rate Constants of Atom Transfer Reactions. *J. Chem. Phys.* **1979**, *83*, 188−199.
(35) Esposito, F.; Capitelli, M.; Gorse, C. Quasi-Classical Dynamics and Vibrational Kinetics of $N + N_2(v)$ system. *Chem. Phys.* **2000**, *257*, 193−202.
(36) Laricchiuta, A.; Pirani, F.; Colonna, G.; Bruno, D.; Gorse, C.; Celiberto, R.; Capitelli, M. Collision Integrals for Interactions Involving Atoms in Electronically Excited States. *J. Phys. Chem. A* **2009**, *113*, 15250−15256.
(37) Capitelli, M.; Bruno, D.; Colonna, G.; Catalfamo, C.; Laricchiuta, A. Thermodynamics and Transport Properties of Thermal Plasmas: the Role of Electronic Excitation. *J. Phys. D: Appl. Phys.* **2009**, *42*, 194005.
(38) Wang, D.; Stallcop, J. R.; Huo, W. M.; Dateo, C. E.; Schwenke, D. W.; Partridge, H. Quantal Study of the Exchange Reaction for $N + N_2$ Using an Ab Initio Potential Energy Surface. *J. Chem. Phys.* **2003**, *118*, 2186−2189.
(39) Esposito, F.; Capitelli, M. QCT Calculations for the Process $N_2(v)+N \rightarrow N_2(v')+N$ in the Whole Vibrational Range. *Chem. Phys. Lett.* **2006**, *418*, 581−585.
(40) Galvão, B. R. L.; Varandas, A. J. C.; Braga, J. P.; Belchior, J. C. Vibrational Energy Transfer in $N(^2D)+N_2$ Collisions: A Quasiclassical Trajectory Study. *Chem. Phys. Lett.* **2013**, *577*, 27−31.
(41) Varandas, A. J. C. Extrapolation Method for Cross-Section from Quantum Mechanical $J = 0$ reactivity: $H + O_2$. *Mol. Phys.* **1995**, *85*, 1159−1164.